Some methods of theoretical modeling of physical properties of pure and doped with transition metal ions functional materials

Mikhail G. Brik

Institute of Physics, University of Tartu, Ravila 14C, Tartu 50411, Estonia

brik@fi.tartu.ee

Introduction

For a long time, unusual properties of crystals with transition metal and rare earth ions have been fascinating physicists and chemists as a non-exhausting source of unsolved puzzles and enigmas, understanding and explanation of which advances our knowledge about matter, helps developing new technologies and gives an esthetic satisfaction to the researchers. An enormous potential of these compounds as new materials has become evident and is not questioned. Applictions in different fields are now established, such as new laser materials, infrared to visible up conversion materials, systems involving photoredox processes for solar energy conversion, new photovoltaic devices, phosphorescent sensors, in particular electroluminescent devices, etc.

All these applications are based on the possibility to add some impurities – other chemical elements – to a crystal lattice. Even a small amount of impurity ions, introduced into the crystal either artificially or naturally, can change drastically its optical properties. A classic example is that one of corundum, or aluminum oxide Al_2O_3. If it is chemically „pure", it appears to be either colorless or greyish crystal. But if it contains a small (about few percent) contribution of chromium ions, corundum changes its color to pink or red, and it becomes a precious stone ruby. If, on the contrary, there are not chromium but titanium and iron additions, the color of corundum is changed to blue and it becomes another precious stone, blue sapphire.

The ability of different materials to absorb and emit light as well as the potetial for possible applications are directly related to the properties of the electronic ground state and the lower-lying excited states of a particular ion in a particular host matrix. It took scientists quite long time to arrive at this conclusion. Thus, the four well-known sharp lines of hydrogen atom in the visible spectral range were a mystery until J.J. Balmer in 1885 suggested an empirical equation, which allowed to calculate the wavelengths of those lines. But an explanation (not a simple description!) should have waited until E. Rutherford and N. Bohr in early XX century developed a planetary model of an atom, which eventually led to creation of quantum mechanics –

a special branch of physics aimed at the proper description of small objects – molecules, atoms, electrons.

An enormous step towards understanding and modeling of optical properties of impurities in crystals was advanced by H. Bethe, when he wrote an article „Splitting of Terms in Crystals" [1]. In this paper he laid down the foundations of the modern crystal field theory; besides, he has given a concise explanation of how the group theory can be applied to the analysis of spectra of impurity ions in crystal field of various symmetry. The further developments in the crystal field theory are linked with the names of J.H. Van Vleck, S. Sugano, Y. Tanabe, D.J. Newman etc.

Those factors, which affect the impurity ion energy level scheme, are as follows: i) electrical charges of the impurity ion and host lattice ions, ii) interionic separations, iii) coordination number (number of the nearest neighboring ions around impurity), symmetry of an environment around impurity etc. In the next section we review briefly the main ideas underlying the quantitative theory of crystal field.

Basic foundations of the crystal field theory

From the quantum mechanical point of view, the energy levels E of an impurity ion with unfilled electron shell, in no relativistic case, can be represented as the solutions of the following Schrödinger equation:

$$\left\{\sum_{i=1}^{n}\left(-\frac{\hbar^2}{2m}\Delta_i + U(\vec{\boldsymbol{r}}_i)\right) + V(\vec{\boldsymbol{r}}_i)\right\}\Psi = \mathrm{E}\Psi \qquad (1)$$

where: $-\frac{\hbar^2}{2m}\Delta_i$ is the kinetic energy of the *i*-th electron with mass m, $U(\vec{\boldsymbol{r}}_i)$ is the potential energy of the *i*-th electron in the electrostatic field created by the impurity ion's nucleus and its remaining electrons and

$$V(\vec{\boldsymbol{r}}_i) = -\sum_{j=1}^{N}\frac{Z_j e^2}{|\vec{\boldsymbol{R}}_j - \vec{\boldsymbol{r}}_i|} \qquad (2)$$

is the potential energy of the *i*-th electron of impurity ion in the electrostatic field created by crystal lattice ions with charges Z_j (in units of the proton charge) with the position vectors $\vec{\boldsymbol{R}}_j \cdot V(\vec{\boldsymbol{r}}_i)$ is the crystal field operator. The summation in Eq. (1) is carried over all electrons in the impurity ion's unfilled shell, and the summation in Eq. (2) is extended over *N* ions of crystal lattice. Eq. (2) is usually solved using the perturbation theory, i.e. assuming that $V(\vec{\boldsymbol{r}}_i) \ll \sum_{i=1}^{n}\left(-\frac{\hbar^2}{2m}\Delta_i + U(\vec{\boldsymbol{r}}_i)\right)$.

The wave functions of the free ion LS-terms (which, actually, are linear combinations of the one-electron wave functions; L and S stand for the orbital and spin momenta of a particular multielectron state, respectively) can be taken as the first approximation, and effects of a small perturbation produced by a crystal field on these free-ion states

will be considered. The matrix elements of the crystal field should be calculated on the wave functions Ψ_n, $\Psi_{n'}$ of free ion as follows:

$$V_{n,n'} = \int \Psi_n^* V(\vec{\boldsymbol{r}})\, \Psi_{n'} dq \tag{3}$$

Integration in the last equation is carried over all spatial coordinates q. The main question now is how to evaluate the integral in Eq. (3). To this end, it is convenient to expand the perturbation operator $V(\vec{\boldsymbol{r}})$ in terms of the spherical harmonics:

$$V(\vec{\boldsymbol{r}}) = \sum_{j=1}^{N} \frac{Z_j e^2}{|\vec{\boldsymbol{R}}_j - \vec{\boldsymbol{r}}|} = Ze^2 \sum_{j=1}^{N} \sum_{k=0}^{\infty} \frac{r_<^k}{r_>^{k+1}} \frac{4\pi}{2k+1} \sum_{m=-k}^{k} Y_{km}(\theta,\varphi) Y_{km}{}^* \left(\theta_j, \varphi_j\right) \tag{4}$$

Here $r_<$ and $r_>$ are the smallest and the greatest of r (electron coordinate) and R_j (distance between the central ion and surrounding point charges), (θ, φ) and $\left(\theta_j, \varphi_j\right)$ are the spherical angular coordinates corresponding to $\vec{\boldsymbol{r}}$ and $\vec{\boldsymbol{R}}_j$ $(j = 1, \ldots, N)$, respectively. At first, it may seem that Eq. (4) does not make the calculation procedure easier at all, although in fact the introduced simplifications are enormous. Although the summation in Eq. (4) is from $k = 0$ to $k = \infty$ (thus implying an infinite number of terms), many terms are vanishing. First of all we note that the matrix elements from Eq. (3) are proportional to the following integrals from the product of three spherical functions

$$V_{n,n'} \sim \int_0^{2\pi} \int_0^{\pi} Y_{l_1 n_1}(\theta,\varphi)^* Y_{km}(\theta,\varphi) Y_{l_2 n'}(\theta,\varphi) sin\theta d\theta d\varphi \tag{5}$$

with quantum numbers l_1 and l_2 being different in general. This integral can be expressed in terms of the Wigner 3*j*-symbols:

$$\int_0^{\pi} \int_0^{2\pi} Y_{l_1 m_1}{}^* Y_{km} Y_{l_2 m_2} sin\theta d\varphi d\theta =$$
$$(-1)^{m_1} \sqrt{\frac{(2l_1+1)(2k+1)(2l_2+1)}{4\pi}} \begin{pmatrix} l_1 & k & l_2 \\ 0 & 0 & 0 \end{pmatrix} \begin{pmatrix} l_1 & k & l_2 \\ -m_1 & m & m_2 \end{pmatrix} \tag{6}$$

The following conditions should be fulfilled in order to make the integral in Eq. (6) non-zero: i) $0 \le k \le (l_1 + l_2)$; ii) k takes only even values from the above specified interval. That is why, for our case of *d*-electrons only the values $k = 0, 2, 4$ should be considered (if, for example, the atoms with *f* electrons are analyzed, only terms with $k = 0, 2, 4, 6$ would be non-zero).

Thus, the crystal field potential can be expressed in terms of the spherical harmonics, and the coefficients of such a combination depend on the positions and charges of ions of crystal lattice. To summarize the above-given mathematcal derivations, we mention here that nowadays it is already a common practice to express the

energy levels of ions with an unfilled electron shell in a crystal field as the eigenvalues of the following crystal field Hamiltonian:

$$H = \sum_{p=0}^{2l} \sum_{k=-p}^{p} B_p^k O_p^k \quad (7)$$

where O_p^k are the linear combinations of irreducible tensor operators acting on the angular parts of the impurity ion wave functions.

It is instructive to note that the second order contribution (with $k = 2$) vanishes if the surrounding ions form an ideal octahedron, tetrahedron, or cube (such a situation is said to represent a cubic crystal field case). However, the second order contribution is not zero in all other cases. Generally speaking, the maximal number of the non-zero terms in Eq. (7) can be 14 and 27 for the *d* and *f* electrons, respectively. The term with $k = 0$ in Eq. (7) is a constant, which does not depend on the electron coordinates and appears in the same manner in all matrix elements. It does not have any influence on the overall energy level scheme other than a simultaneous shift of all energy levels and, therefore, can be omitted without any lack of generality.

It should be pointed out that several definitions and normalizations of operators O_p^k can be found in the literature [2]. To be consistent, in what follows, we shall use the Stevens' normalization [3]. The B_p^k entries in Eq. (7) are the crystal field parameters (CFP) containing all information about the geometrical structure around impurity center.

There are two different (actually, opposite) ways of determination of the B_p^k values. The first one is to extract their values from fitting the calculated energy levels to the experimentally deduced ones. Such a method is merely a mathematical approach; it is based on the non-linear least square fitting procedures. Nevertheless, in this case one has, first of all, to assume the symmetry of a considered impurity center to identify which CFP are not zero and are then allowed to vary freely. The final set of the CFP obtained as a result of the fitting procedure may be not unique, since it is always possible to be trapped in a local minimum for minimization, which may lead to a wrong crystal field parameterization and, finally, not proper description of the impurity ion energy levels.

The second method is based on a *direct calculation* of the CFP values using the crystal structure data (using as few fitting parameters as possible). Then the calculated CFP are used to diagonalize the crystal field Hamiltonian and compare the obtained energy levels with the experimental spectra. This is more physically based approach, since no initial assumptions about the symmetry of an impurity center are needed, and the calculations start from the available crystal structure data. A small number of the fitting parameters allow for meaningful treatment of the symmetry effects on the impurity ion energy level scheme and comparison of the CFP sets for different ions/different crystals. One of the first methods of this kind was the superposition model (SM) of crystal field [4, 5]. This model is based on the assumptions that only the nearest neighbors (ligands) determine the crystal field around an impurity ion and interaction between each ligand and impurity is axial-symmetric. The

number of the SM parameters is 4 for 3d ions and 6 for 4f ions. For further details of this model, the reader can look into many original publications [6].

A further development of the SM was proposed by B.Z. Malkin [7]. He suggested representing the CFP B_p^k as a sum of two terms:

$$B_p^k = B_{p,q}^k + B_{p,S}^k \tag{8}$$

The first contribution is due to the electrostatic interaction between optical electrons of an impurity ion and ions of crystal lattice (which are considered as the point charges located at the crystal lattice sites, without taking into account their electron structure), and the second one is proportional to the overlap of the wave functions of an impurity ion and ligands. This term takes into account all effects of the covalent bond formation and exchange interaction. Inclusion of these effects significantly improves an agreement between the calculated and experimentally observed energy levels. The expression for calculating the first contribution to the total CFP in the case of a 3*d*-ion is as follows:

$$B_{p,q}^k = -K_p^k e^2 \langle r^p \rangle \sum_i q_i \frac{V_p^k(\theta_i,\varphi_i)}{R_i^{p+1}} \tag{9}$$

The sums are carried out over lattice ions denoted by i with charges q_i, $R_i, \theta_i, \varphi_i$are the spherical coordinates of the i-th ion of crystal lattice in the system of reference centered at the impurity ion. The averaged values $\langle r^p \rangle$ of p-th power of the impurity ion electrons coordinate can be either found in the literature, or calculated numerically using the corresponding ions' wave functions. The values of the numerical factors K_p^k and expressions for the polynomials V_p^k can be all found in the original paper [7]. The second term in Eq. (8) can be calculated as follows:

$$B_{p,S}^k = K_p^k e^2 \frac{2(2p+1)}{5} \sum_i \left(G_S S(s)_i^2 + G_\sigma S(\sigma)_i^2 + \gamma_p G_\pi S(\pi)_i^2 \right) \frac{V_p^k(\theta_i,\varphi_i)}{R_i} \tag{10}$$

The overlap integrals between d-functions of the central ion and p- and s-functions of the ligands are denoted by S_s, S_σ, S_π (they correspond to the following integrals (in the $\langle lm|l'm' \rangle$ notation): $S(s) = \langle d0|s0 \rangle$, $S(\sigma) = \langle d0|p0 \rangle$, $S(\pi) = \langle d1|p1 \rangle$. The G_s, G_σ, G_π entries are dimensionless adjustable parameters of the model, which are determined from the positions of the first three absorption bands. Very often they can be assumed to be equal to each other: $G_s = G_\sigma = G_\pi = G$ (in this case only the first absorption band is required to determine the value of G), and in this paper we use this simplified model. The numerical factor γ_p in the case of d-electrons is $\gamma_2 = 1$ and $\gamma_4 = -4/3$.

The operators O_p^k are the Stevens homogeneous spherical polynomials and are expressed in terms of the spherical operators $C_p^k = \sqrt{\frac{4\pi}{2p+1}} Y_{pk}$ (Y_{pk} are the spherical functions) as follows:

$$O_p^k = \frac{1}{\alpha_{pk}} Z_p^k \tag{11}$$

and Z_p^k are the real tesseral harmonics

$$Z_p^k = \begin{cases} C_p^{-k} + (-1)^k C_p^k, k > 0 \\ C_p^k, k = 0 \\ -i\left(C_p^{-k} - (-1)^k C_p^k\right), k < 0 \end{cases} \tag{12}$$

As we have already mentioned, the maximum number of terms in Eq. (7) is 14 for d-ions, and 27 for f-ions (in this case 13 terms with p = 6 are added). However, the number of non-zero CFP can be reduced significantly if the symmetry of the considered complex is high enough. Thus, in the case of perfect cubic symmetry only two parameters survive in Eq. (7): B_4^0 and $B_4^4 = 5B_4^0$. This significantly simplifies diagonalization of the crystal field Hamiltonian, which can even be done analytically in many cases.

The exchange charge model can be also successfully applied not only to the analysis of the energy levels and absorption spectra of 3d ions in crystals, but to the estimations of the parameters of the electron-vibrational interaction and probabilities of the non-radiative transitions as well [8, 9]. The exchange charge model also has been successfully used for description of the spectra of rare-earth ions in crystals [10-12]. More examples related to 3d ions can be found in a recently published book [13].

Density functional theory

The crystal field theory, although capable of calculating impurity ions energy levels (as will be shown below), can not get a handle on proper description of the energetic band structure of solids. This can be efficiently managed by the density functional theory (DFT), which is a widely used branch of quantum-chemical methods which is based on Hohenberg-Kohn theorems [14, 15].

In a simplistic form the first theorem states that the ground state energy from the Schrödinger equation is a unique functional of the electron density:

$$\rho(\boldsymbol{r}) = 2\sum_{i=1}^{N} \psi_i^*(\boldsymbol{r})\psi_i(\boldsymbol{r}) \tag{13}$$

which is expressed in terms of the one-electron wave functions $\psi_i(\boldsymbol{r})$. The pre-multiplier of 2 appears in front of the summation sign because of the electron's spin. Another way of stating the same theorem is to say that the ground-state electron

density uniquely determines all properties of a ground state, including its energy and wave function. An essential result of this theorem is that it allows to reduce finding solution of the Schrödinger equation with 3N variables to simply finding a suitable function of three spatial variable, which describe the electron density distribution, and which then, by virtue of the first Hohenberg-Kohn theorem, will provide exact description of the system's ground state.

At the same time, the first Hohenberg-Kohn theorem postulating existence of the electron density functional says nothing about what this functional looks like. This is the second Hohenberg-Kohn theorem, which gives a key to the choice of the electron density functional: the electron density that minimizes the energy of the overall functional is the true electron density corresponding to the full solution of the Schrödinger equation.

If the „true" functional were known, the electron density could be varied until reaching the energy minimum. This variational principle forms the key stone of application of these two theorems. The energy functional can be written as:

$$E[\![\psi_i]\!] = E_{known}[\![\psi_i]\!] + E_{XC}[\![\psi_i]\!] \tag{14}$$

where $\psi_i$is the one-electron wave function, the first term in the right-hand side represents all "known" terms containing the kinetic and potential energies of all electrons and nuclei in the considered system, and all everything else is hidden in the second term of the right-hand side, also known as the exchange-correlation functional.

Kohn and Sham have shown that the right electron density can be found by solving a set of the one-electron equations, each of which involves only one electron and is very similar to the Schrödinger equation:

$$\left[-\frac{\hbar^2}{2m}\Delta^2 + V(\boldsymbol{r}) + V_H(\boldsymbol{r}) + V_{XC}(\boldsymbol{r})\right]\psi_i(\boldsymbol{r}) = \varepsilon_i\psi_i(\boldsymbol{r}) \tag{15}$$

with:

$$V_H(\boldsymbol{r}) = e^2\int\frac{\rho(\boldsymbol{r'})}{|\boldsymbol{r}-\boldsymbol{r'}|}d^3\boldsymbol{r'} \tag{16}$$

being the Hartree potential. It describes the Coulomb repulsion between that electron which is considered in one of the Kohn-Sham equations and the total electron density defined by all electrons in the system. It also incorporates the so-called self-interaction, because the considered electron also contributes to the formation of the total electron density. Therefore, it describes, in other words, the Coulomb interaction between the electron and itself, which is an unphysical interaction, of course. The correction for such an unphysical interaction is also included into the exchange-correlation potential $V_{XC}(\boldsymbol{r})$**,** which is defined as the functional derivative of the exchange-correlation energy:

$$V_{XC}(\boldsymbol{r}) = \frac{\delta E_{XC}(\boldsymbol{r})}{\delta \rho(\boldsymbol{r})} \tag{17}$$

Here the functional derivative (which, strictly speaking, is not equal to the functions's derivative) is shown by symbol δ.

It can be seen that the electron density $\rho(\boldsymbol{r})$ enters the Hartree potential. At the same time, it is a key-variable to determine the exchange-correlation potential $V_{XC}(\boldsymbol{r})$. To find an exit from this locked circle, the following algorithm is applied:

1) An initial (trial) electron density $\rho(\boldsymbol{r})$ is defined. It can be a "good guess" or an already known density for a similar system.
2) The Kohn-Sham equations are solved with this trial density to find the single-electron wave functions $\psi_i(\boldsymbol{r})$.
3) The electron density $\rho(\boldsymbol{r})$ is calculated with *those* $\psi_i(\boldsymbol{r})$.
4) The calculated in step 3 electron density is compared with that one used in step 1. If these two densities are identical, the ground state electron density is found and it can be used to calculate the total energy of a system etc. If these two densities are different, than the trial density should be updated and the whole procedure is repeated until the difference between the two electron densities from two consecutive iteration procedures will not exceed an earlier chosen accuracy limit.

After we have "set the stage" by having shortly described the basic foundations of the crystal field theory and DFT, we continue with several examples of application of these calculating techniques to some real physical systems.

Example of application of the exchange charge model: Mn^{5+} ions in Li_3PO_4, Ca_2PO_4Cl and $Sr_5(PO_4)_3Cl$ crystals

Crystals doped with transition metal ions having $3d^2$ external electronic configuration, V^{3+}, Cr^{4+}, Mn^{5+}, Fe^{6+}, etc., are of interest for applications as solid-state laser active media [13]. These ions usually lie in sites having tetrahedral oxygen coordination either with low (V^{3+}, Cr^{4+}) or strong (Mn^{5+}, Fe^{6+}) crystal field. In the former case the broadband emission from the $^3T_2$ state in the near infrared spectral region is attractive for tunable laser application, whereas in the latter the emission from the ^1E level consists mainly of a sharp feature suitable for laser action only in some favourable host lattices. The analysis of the energy level structure of these dopants in suitable hosts is then important in order to assess their perspective applications. In this section we show how the exchange charge model can be applied to the comparative analysis of the low temperature absorption spectra of the Mn^{5+} ion in Li_3PO_4, Ca_2PO_4Cl and $Sr_5(PO_4)_3Cl$ crystals [16]. Using the exchange charge model, as described in section 2, we calculated the crystal field parameters acting on the Mn^{5+} ions in all chosen hosts and the Mn^{5+} energy levels, which were compared with the experimental absorption spectra shown in Figs. 1-3.

The main message which can be taken from Figs. 1-3 is that all peaks in the experimental absorption spectra (solid lines) can be given an exact assignment in terms of the Mn^{5+} energy levels split in the tetrahedral crystal field. All notations in the figures are standard ones in the crystal field theory and are based on the irreducible representations of the T_d point group. Without going into fine details of the performed calculations, we note that the experimentally observed maxima of absorption are in very good agreement with the calculated Mn^{5+} energy levels. Moreover, the structure of the absorption peaks is perfectly accounted for by the low-symmetry splitting of the orbitally degenerated states of manganese ions. Comparison of the calculated splittings of the $^3T_1$ states at about 16000-18000 cm^{-1} allowed to find the following trend of symmetry lowering of the MnO_4 units: Li_3PO_4 (highest symmetry – smallest splitting) → $Sr_5(PO_4)_3Cl$ (intermediate case – intermediate splitting) → Ca_2PO_4Cl (lowest symmetry – highest splitting). Such a behavior was found to be in line with increase of the second rank crystal field invariants in the same direction. The performed calculations together with low-temperature spectroscopic studies of these three materials helped remove some earlier existing ambiguities in interpretation of their optical spectra [16].

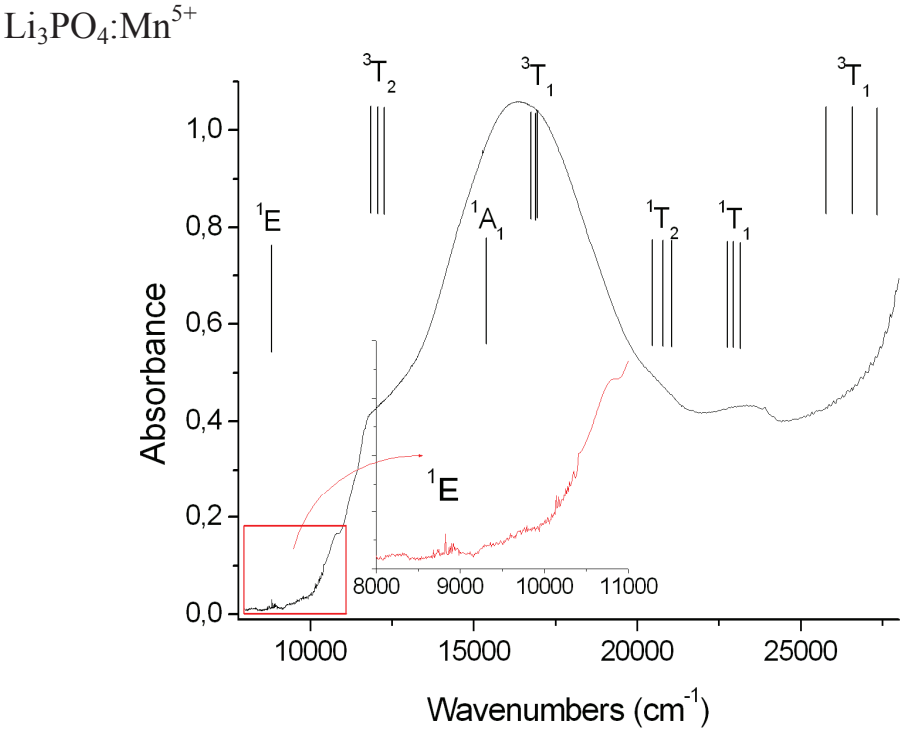

Fig. 1. 10 K unpolarized absorption spectrum of $Li_3PO_4:Mn^{5+}$. The calculated Mn^{5+} energy levels are shown by vertical lines.

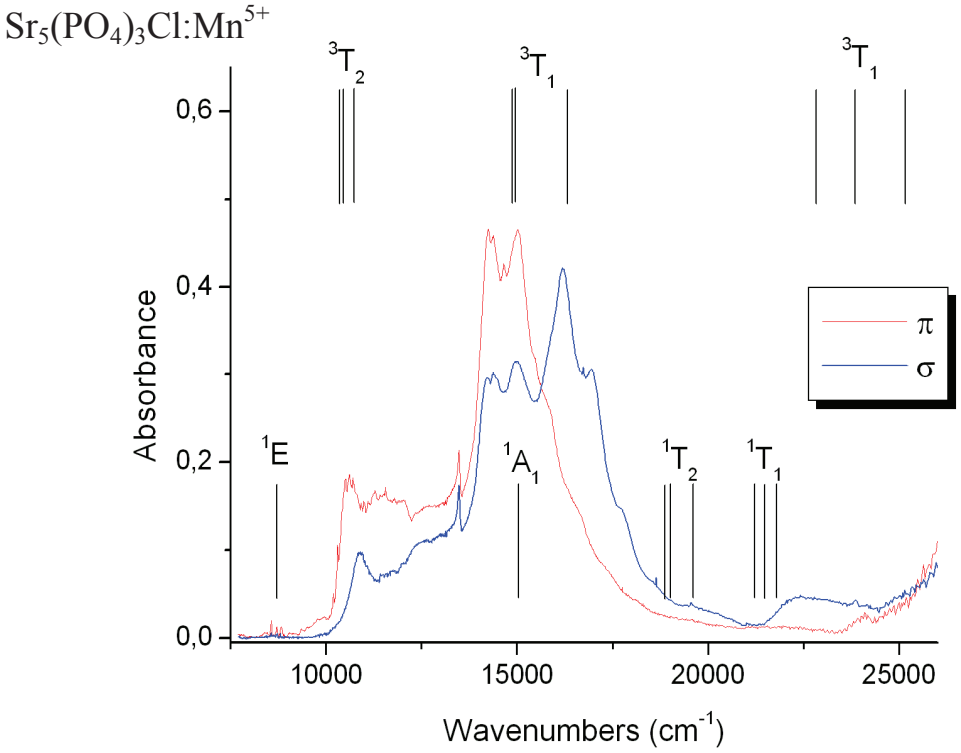

Fig. 2. 10 K polarized absorption spectrum of $Sr_5(PO_4)_3Cl:Mn^{5+}$. The calculated Mn^{5+} energy levels are represented as vertical lines.

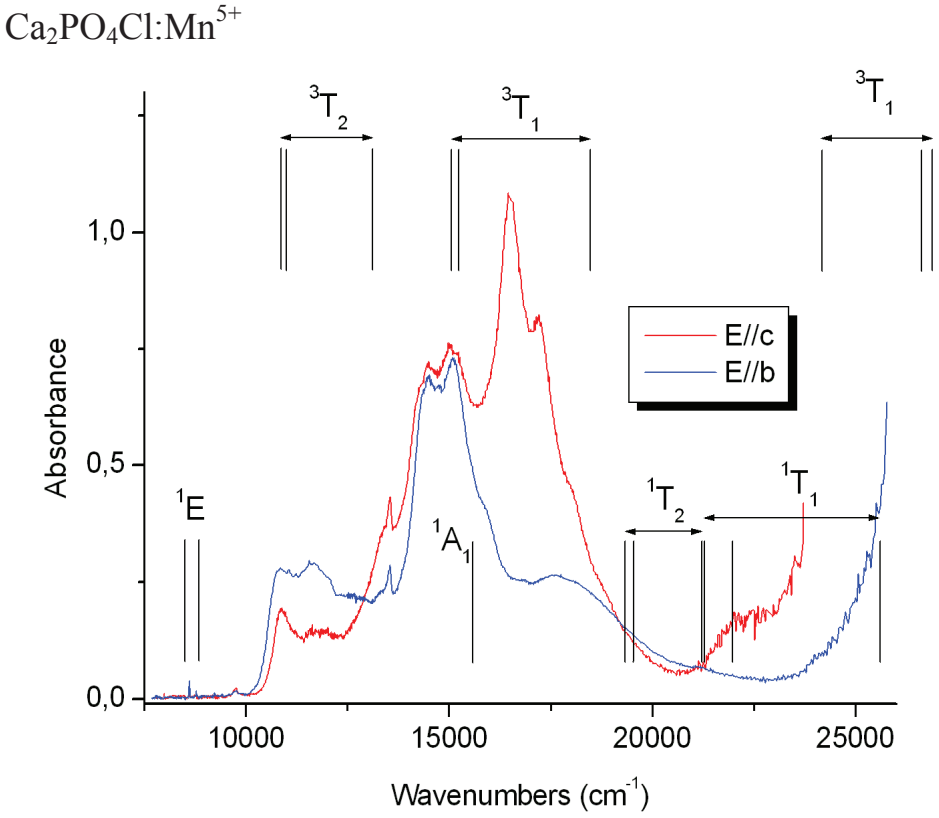

Fig. 3. 10 K polarized absorption spectrum of $Ca_2PO_4Cl:Mn^{5+}$. The calculated Mn^{5+} energy levels are shown by vertical lines.

Example of ab initio analysis of the optical and elastic properties of crystals: $ZnWO_4$, $CdWO_4$ and transition metal monocarbides

First-principles calculations of the structural, electronic, optical and elastic properties of crystals become now an indispensable tool for search for new materials and careful explanation of the properties of already existing ones.

In particular, recently we have studied in details two technologically important crystals – $CdWO_4$ and $ZnWO_4$ – which are used as scintillator materials [17]. The calculations were performed using the CASTEP module [18] of the Materials Studio package; all the necessary details can be found in the above-cited paper. As an illustration of the obtained results, we show here the calculated band structures of both materials (Fig. 4), obtained by employing the general gradient approximation (GGA) and local density approximation (LDA).

As seen from Fig. 2, electronic states exhibit considerable dispersion, to a larger extent in the conduction band (CB) and to a smaller extent in the valence band (VB), which is indicative of significant anisotropy of the effective masses of the charge carriers (and thus electric conductivity) in both crystals along various directions in the **k**-space. The lowest part of the CB in $CdWO_4$ consists of the tungsten 5d, whereas the cadmium 5s states contribute to its upper part. The oxygen 2p states are mixed with the Cd and W states and thus can be also seen in the CB. The lowest part of the VB is composed of the well-localized Cd 4d states. The W 5d and O 2p states form the top part of the VB.

In $ZnWO_4$ the CB displays two clearly separated sub-bands. The lower one (from ~ 5 to 6 eV) is basically due to the W 5d states, while the upper one (from 7 to 11 eV) is formed by the Zn 4s states. A small contribution originating from the O 2p states hybridized with the metal states can be also traced down in the CB. The Zn 3d states are spread over the whole VB, with a well-pronounced maximum at about -5 eV. The oxygen 2p states form the upper part of the VB along with the W 5d states slightly contributing to the VB due to the hybridization effects.

An experimental verification of the calculated electronic structure comes from the X-ray photoelectron spectroscopy (XPS). Fig. 5 shows the comparison between the theoretical DOS diagrams obtained in the present work and experimental XPS spectra [19].

The low-energy XPS peak at about 1 eV in Fig. 5 is mainly due to the O 2p states in both crystals. A minor contribution of the Zn 3d states to this peak is noticeable in $ZnWO_4$, while the contribution the Cd 4d states at this energy is substantially smaller in $CdWO_4$. The contributions of the W 5d states applied only to the lowest XPS peaks and were considered practically identical for $CdWO_4$ and $ZnWO_4$ [19]. However, they are different in our case. The presence of the W 5d states in the lowest XPS peak is non-negligible in $CdWO_4$, whereas in $ZnWO_4$, they mainly contribute to the second XPS peak at about 5 eV. This second, most intensive peak located at about 6 eV in $CdWO_4$ and 5 eV in $ZnWO_4$ is mainly due to the Cd 4d (Zn 3d) states, respectively.

The third experimental XPS peak at about 16-17 eV is basically due to the oxygen 2s states, with a smaller but still distinct contribution from the W 5d states due to the hybridization of the latter with the O states. So, these calculations of electronic properties allowed to explain completely the experimental XPS spectra.

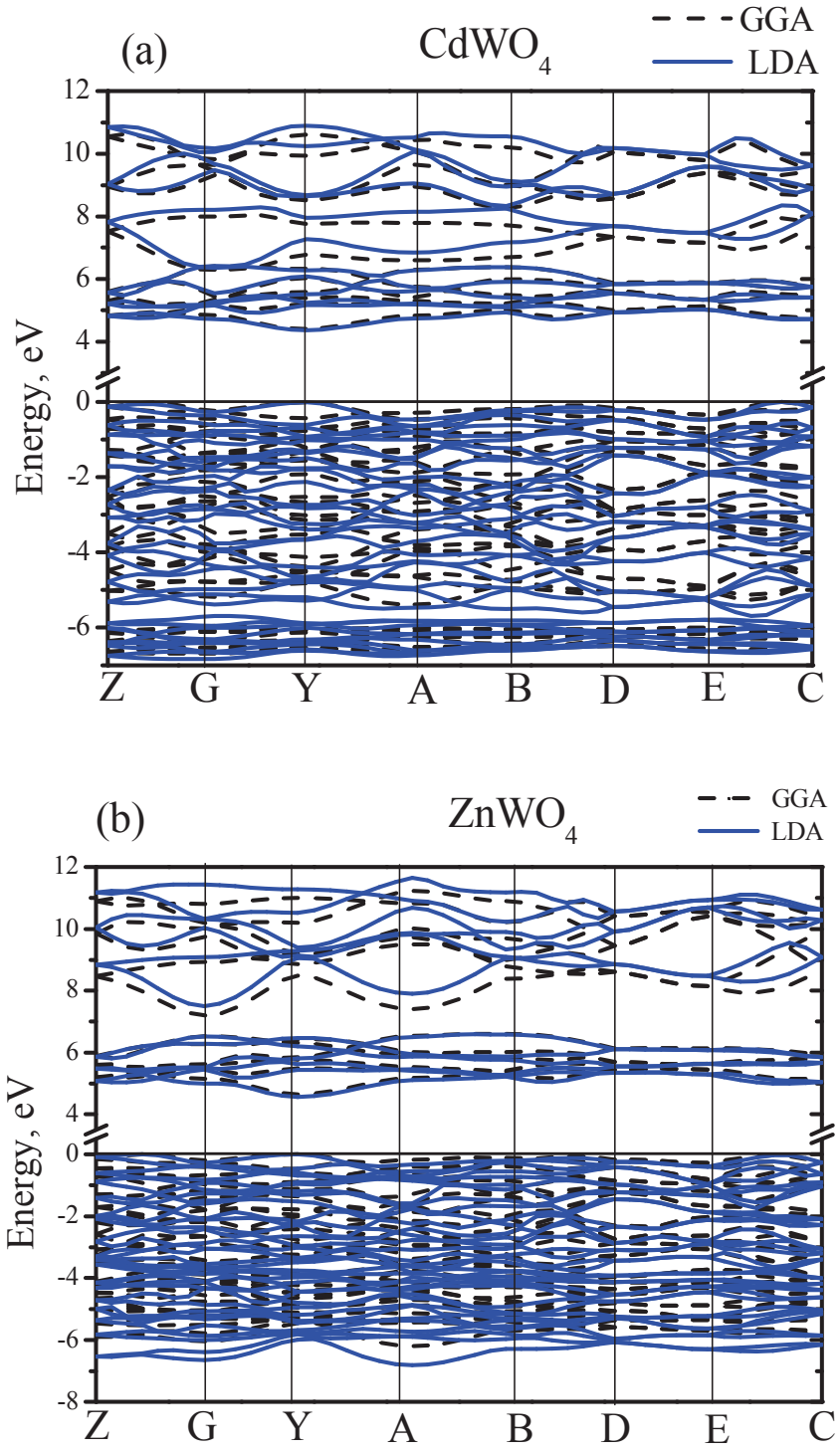

Fig. 4. Band structures calculated for $CdWO_4$ (a) and $ZnWO_4$ (b). The LDA and GGA results are shown by the solid and dashed lines, respectively.

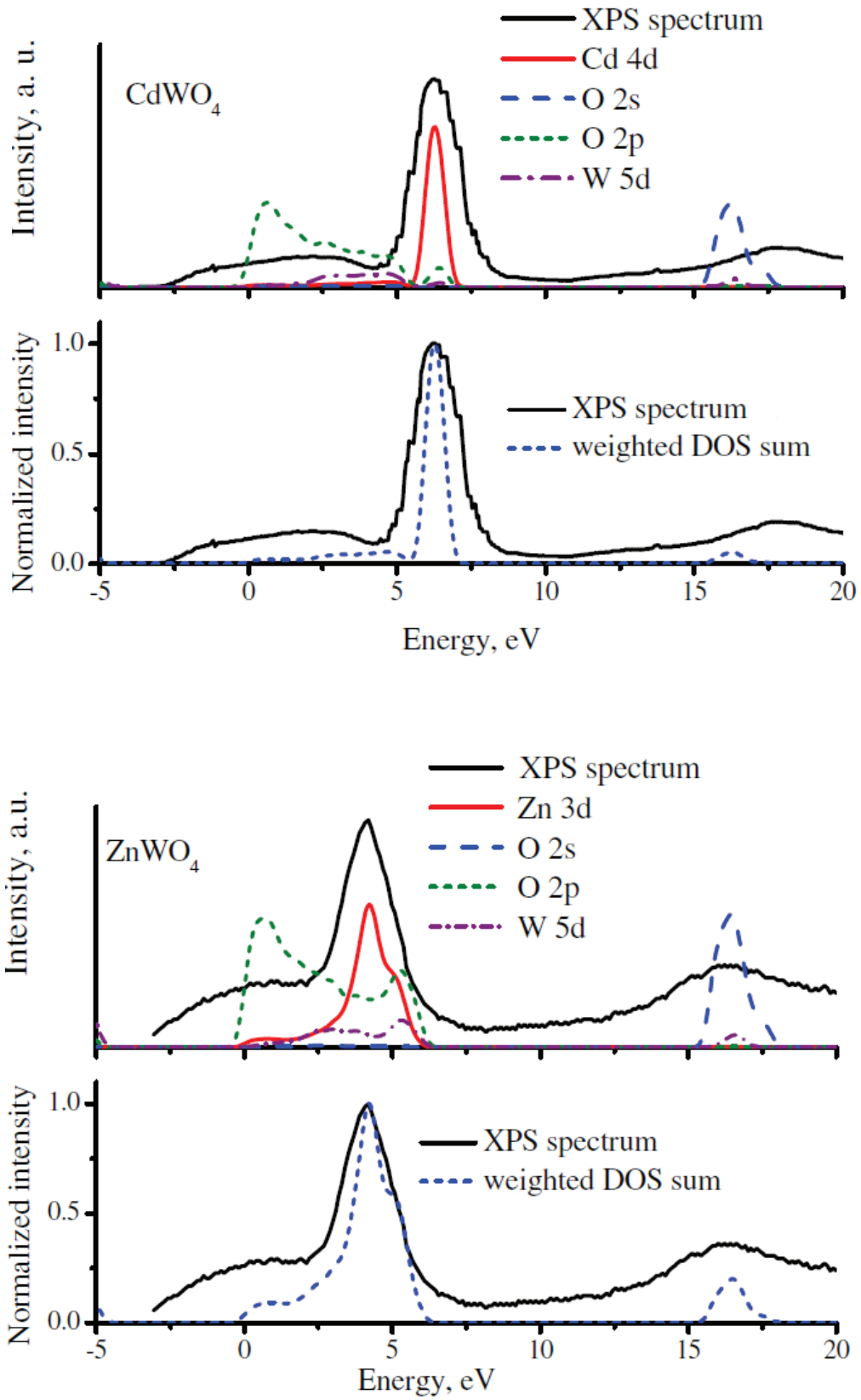

Fig. 5. Comparison of experimental XPS spectra [19] and partial density of states (DOS) diagrams for $CdWO_4$ and $ZnWO_4$.

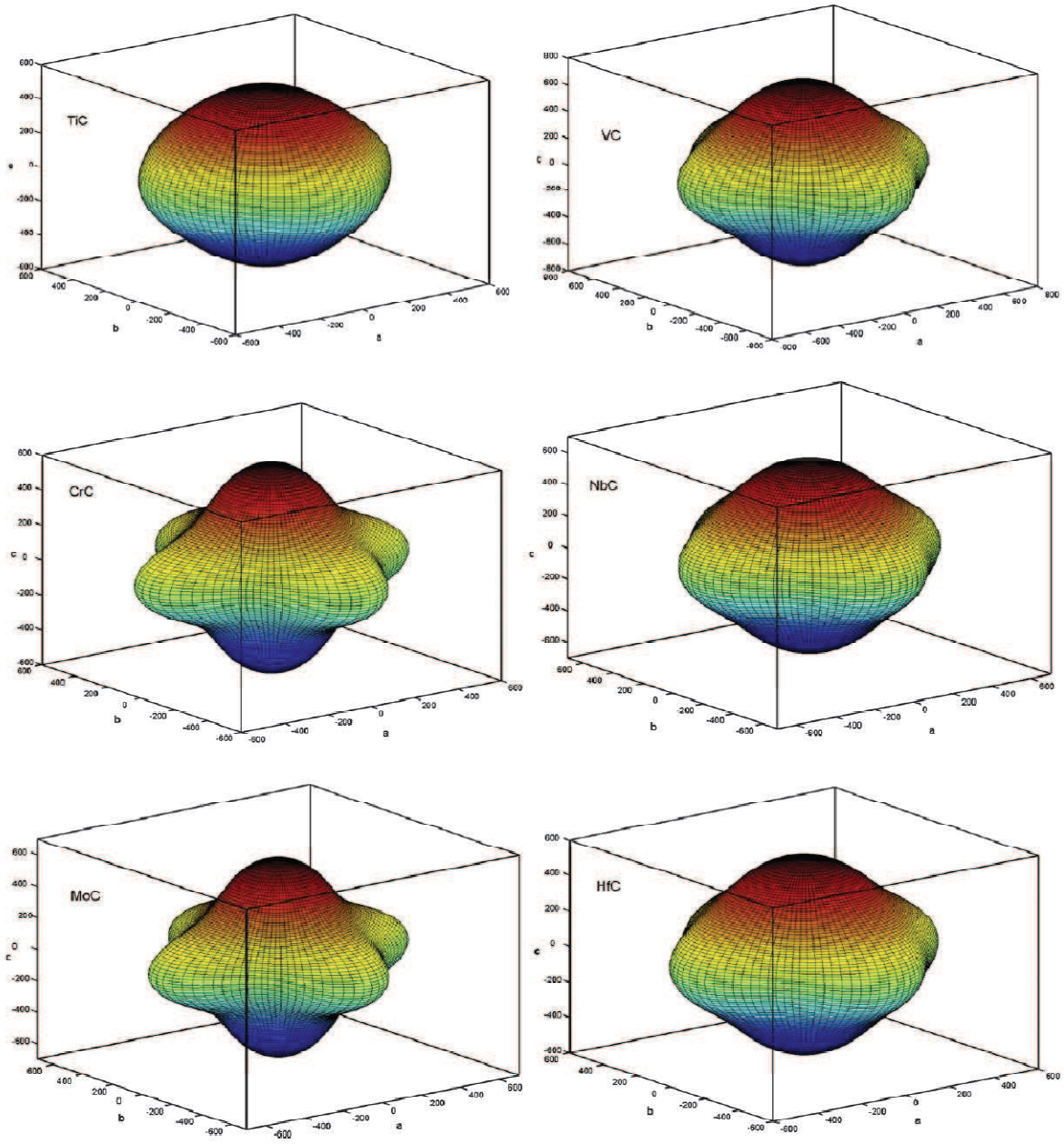

Fig. 6. Directional dependence of the Young's moduli for ScN, TiN, VN, CrN, ZrN and NbN. The GGA results were used for plotting all surfaces and cross-sections. The axes units are GPa.

Another important application of the ab initio calculations is an analysis of the elastic properties of solids. As an illustration of such consideration, we show in Fig. 6 the three-dimensional visualisation of the Young's moduli in six transition metal monocarbides: TiC, VC, CrC, NbC, MoC, and HfC [20]. These materials have unique combination of high hardness, high melting point and conductivity, which makes them to be suitable for many technological applications, i.e. coating, corrosion resistance on machine tooling etc. The meaning of these figures is as follows: the distance from the center of those figures to the surface is equal to the Young's modulus along a chosen direction in a crystal lattice.

The main conclusion which can be drawn up from the shown figures is as follows: all compounds are elastically anisotropic; in other words, they react in different ways to the stresses applied along different directions. In particular, CrC exhibits remarkable anisotropy: it is a very hard material if the stress is applied along the crystallographic axis, and turns out to be fragile if the stress is applied along any other direction. Such a circumstance undoubtedly imposes certain limitations to the use of CrC as a coating material, for example, or as a part of machines and rotating tools.

Combination of semi-empirical and ab initio methods of analysis of optical properties of doped crystals: $ZnAl_2S_4:Co^{2+}$ crystals

$ZnAl_2S_4$ is a „classical" representative of a large group of spinel crystals. Its structure is such that it can be easily doped with transition metal ions. In particular, Co^{2+} ions can occupy the Zn^{2+} sites, surrounded by four sulfur ions.

We performed a combined analysis (employing the exchange charge model of crystal field and CASTEP module of Materials Studio) of the spectroscopic properties of $ZnAl_2S_4:Co^{2+}$ [21]. The main results of these studies are summarized in Figs. 7 and 8.

As Fig. 7 shows, the CASTEP calculated absorption spectrum reproduces well the basic features of the experimental spectrum. In addition, the calculated (using the exchange charge model) energy levels of trivalent vanadium are in very good agreement with positions of the experimental absorption bands maxima.

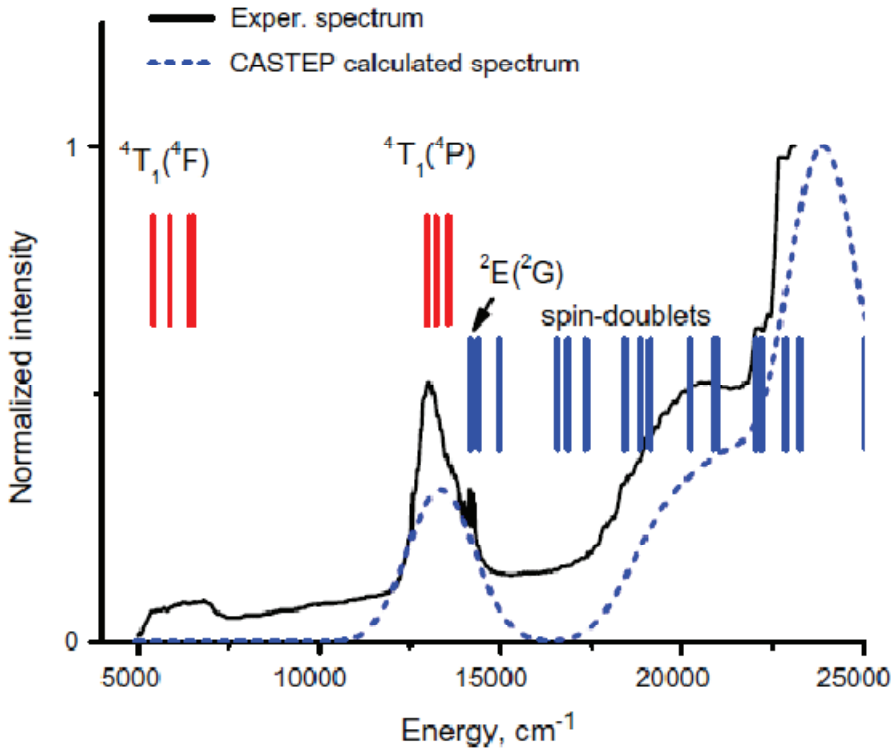

Fig. 7. Comparison between the experimental (solid line), *ab initio* calculated (dashed line) absorption spectra of $ZnAl_2S_4:Co^{2+}$ and calculated (crystal field theory, vertical lines) energy levels of Co^{2+}.

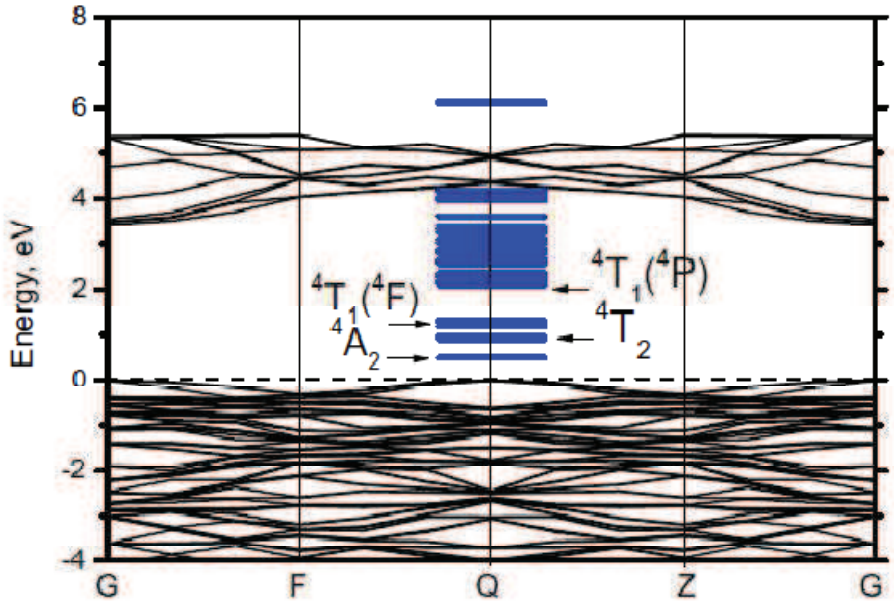

Fig. 8. The calculated band structure of $ZnAl_2S_4$ with superimposed energy levels of Co^{2+} ions.

Finally, combination of the ab initio calculated electronic structure with the results of the vanadium energy levels calculations allows to draw the complete energy level structure of $ZnAl_2S_4$:Co^{2+} (Fig. 8), which includes the host's band structure and impurity energy levels superimposed onto it. The key result here is that the position of the lowest energy level of Co^{2+} impurity in the $ZnAl_2S_4$ band gap was established to be located at about 0.5 eV above the top of the valence band.

Conclusions

We have shown several examples of how the semi-empirical crystal field analysis, based on the exchange charge model of crystal field, and DFT-based first principles calculations of the structural, electronic, optical and elastic properties can be combined together to gain a complementary picture of the physical properties of crystals doped with the transition metal and rare earth ions. An interested reader is kindly advised to read the articles cited in the list of references.

Acknowledgments

This research was supported by i) European Social Fund's Doctoral Studies and Internationalisation Programme DoRa; ii) European Union through the European Regional Development Fund (Center of Excellence „Mesosystems: Theory and Applications", TK114); iii) bilateral agreements between the Estonian and Polish Academies of Sciences in the years 2010-2015.

References

[1] H.A. Bethe, *Splitting of Terms in Crystals*, Ann. Physik 3 (1929) 133-206.

[2] C. Rudowicz, *Transformation relations for the conventional O_k^q and normalized $O_k'^q$ Stevens operator equivalents with k = 1 to 6 and -k ≤ q ≤ k*, J. Phys. C: Solid State Phys. 18 (1985) 1415-1430.
[3] K.W.H. Stevens, *Matrix Elements and Operator Equivalents Connected with the Magnetic Properties of Rare Earth Ions,* Proc. Phys. Soc. A, 65 (1952) 209.
[4] D.J. Newman, *Theory of lanthanide crystal fields*. Adv. Phys. 20 (1971) 197-256.
[5] D.J. Newman, B. Ng, *The superposition model of crystal fields*, Rep. Prog. Phys. 52 (1989) 699.
[6] Y.Y. Yeung, *Superposition model and its applications*, in: Optical Properties of 3d-ions in Crystals: Spectroscopy and Crystal Field Analysis, Eds. N.M. Avram and M.G. Brik (Springer, Tsinghua University Press, 2013), p. 95-121.
[7] B.Z. Malkin, *Crystal field and Electron-Phonon Interaction in Rare-Earth Ionic Paramagnets, in: Spectroscopy of Solids Containing Rare-Earth Ions*, Eds. A.A. Kaplyanskii and B.M. Macfarlane (Amsterdam: North Holland, 1987), p. 33-50.
[8] A.G. Avanesov, M.G. Brik, E.N. Tumayev, *Non-radiative transitions in the oscillating field model*. J. Lumin., 92 (2001) 133-137.
[9] M.G. Brik, G.E. Drăgănescu, N.M. Avram, C.N. Avram, *Non-radiative transitions in the anharmonic oscillating field model*, Physica B: Condensed Matter, 364 (2005) 170-179.
[10] D.S. Pytalev, E.P. Chukalina, M.N. Popova, G.S. Shakurov, B.Z. Malkin, S.L. Korableva, *Hyperfine interactions of Ho^{3+} ions in KY_3F_{10}: Electron paramagnetic resonance and optical spectroscopy studies*, Phys. Rev. B 86 (2012) 115124.
[11] V.N. Makhov, M. Kirm, G. Stryganyuk, S. Vielhauer, G. Zimmerer, B.Z. Malkin, O.V. Solovyev, S.L. Korableva, *5d-4f luminescence of Ce^{3+}, Gd^{3+} and Lu^{3+} in $LiCaAlF_6$*, J. Lumin. 132 (2012) 418-424.
[12] M.G. Brik, I. Sildos, V. Kiisk, *Calculations of physical properties of pure and doped crystals: Ab initio and semi-empirical methods in application to $YAlO_3$:Ce^{3+} and TiO_2*, J. Lumin. 131 (2011) 396-403.
[13] M.G. Brik, N.M. Avram, C.N. Avram, *Exchange charge model of crystal field for 3d ions, in: Optical Properties of 3d-ions in Crystals: Spectroscopy and Crystal Field Analysis*, Eds. N.M. Avram and M.G. Brik (Springer, Tsinghua University Press, 2013), p. 29-94
[14] P. Hohenberg, W. Kohn, *Inhomogeneous Electron Gas,* Phys. Rev. 136 (1964) B864-B871.
[15] W. Kohn, L.J. Sham, *Self-Consistent Equations Including Exchange and Correlation Effects,* Phys. Rev. 140 (1965) A1133-A1138.
[16] M.G. Brik, E. Cavalli, R. Borromei, M. Bettinelli, *Crystal field parameters and energy level structure of the MnO_4^{3-} tetroxo anion in Li_3PO_4, Ca_2PO_4Cl and $Sr_5(PO_4)_3Cl$ crystals,* J. Lumin. 129 (2009) 801-806.
[17] M.G. Brik, V. Nagirnyi, M. Kirm, *Ab-initio studies of the electronic and optical properties of $ZnWO_4$ and $CdWO_4$ single crystals*, Mater. Chem. Phys. 134 (2012) 1113-1120.
[18] M.D. Segall, P.J.D. Lindan, M.J. Probert, C.J. Pickard, P.J. Hasnip, S.J. Clark, M.C. Payne, *First-principles simulation: ideas, illustrations and the CASTEP code*, J. Phys. Condens. Matt. 14 (2012) 2717.
[19] M. Itoh, N. Fujita, Y. Inabe, *X-ray photoelectron spectroscopy and electronic structures of scheelite- and wolframite-type tungstate crystals*, J. Phys. Soc. Jpn. 75 (2006) 084705.
[20] V. Krasnenko, M.G. Brik, *First-principles calculations of hydrostatic pressure effects on the structural, elastic and thermodynamic properties of cubic monocarbides XC (X = Ti, V, Cr, Nb, Mo, Hf)*, Solid State Sci. 14 (2012) 1431-1444.
[21] M.G. Brik, M. Nazarov, M.N. Ahmad-Fauzi, L. Kulyuk, S. Anghel, K. Sushkevich, G. Boulon, *Comparative first-principles analysis of un-doped and Co^{2+}-doped α-$ZnAl_2S_4$*. J. Alloys Compd. 550 (2013) 103-108.